FOCUS ISSUE OF SELECTED PAPERS FROM IMLB 2016 WITH INVITED PAPERS CELEBRATING 25 YEARS OF LITHIUM ION BATTERIES

Investigation into State-of-Health Impedance Diagnostic for 26650 4P1S Battery Packs

B. M. Huhman,[a,*,z] J. M. Heinzel,[b] L. Mili,[c] C. T. Love,[d,] and D. A. Wetz[e,**]**

[a]*Plasma Physics Division, US Naval Research Laboratory, Washington, DC 20375, USA*
[b]*Naval Surface Warfare Center, Philadelphia, Pennsylvania 19112, USA*
[c]*Bradly Dept. of Electrical Engineering, Virginia Tech, Blacksburg, Virginia 24061, USA*
[d]*Chemistry Division, US Naval Research Laboratory, Washington, DC 20375, USA*
[e]*Department of Electrical Engineering, University of Texas - Arlington, Arlington, Texas 76019, USA*

State-of-Health (SoH) is a critical parameter for determining the safe operating area of a battery cell and battery packs to avoid abuse and prevent failure and accidents. Experiments were performed at the US Naval Research Laboratory (NRL) on a 4P1S cell array using pulsed discharge and electrochemical impedance spectra (EIS) to determine a single-point SoH frequency for the array as a whole. Individual cell EIS measurements were taken, as well as measurements of the array as a whole. This work will discuss experimental results to date.

Manuscript submitted September 14, 2016; revised manuscript received January 10, 2017. Published January 24, 2017. This was Paper 656 presented at the Chicago, Illinois, Meeting of the IMLB, June 19–24, 2016. *This paper is part of the Focus Issue of Selected Papers from IMLB 2016 with Invited Papers Celebrating 25 Years of Lithium Ion Batteries.*

The US Navy is currently developing a host of electrical systems that rely on high pulsed power for their operation. In pulsed power supplies, energy is slowly, over several milliseconds to several seconds in most cases, transferred from an energy dense prime power supply into some intermediate power dense storage device, which is then able to release the energy in the form of a high peak to average power pulse to the load. In a laboratory setting, grid-tied power supplies are often used as the prime power supply. Aboard a mobile platform, the necessary power must be carried with the pulsed power system, which will have a limited lifetime and performance envelope. In recent years, lithium-ion batteries have emerged as a key component to the development of compact, portable pulsed-power devices because they can be engineered to be either energy dense or power dense. In the vast majority of pulsed power systems, the intermediate energy storage device is a large capacitor that is charged at a relatively slow rate prior to the rapid discharge of high current into the load under test. This method has the advantage of always allowing us to know whether the input energy magnitude and quality are suitable for the application. A limited power supply requires care in the system design to ensure sufficient power is available to be delivered to the capacitive load.

Unlike many battery-driven loads, such as electric vehicles, pulsed power systems require much higher power output in a short amount of time meaning that in most cases, power cells are being considered rather than energy cells. In order to meet the power and capacity requirements, multiple cells will be connected in series to generate a sufficient potential to drive the load. Oversizing the battery by putting more cells in parallel than are needed will reduce the current supplied by each cell and will increase their lifetime. Here, it is assumed that each parallel cell equally shares the current demanded by the load, though in most cases the manner in which the batteries are paralleled prevents verification that this current sharing does occur. In the Navy's applications, size and weight are critical; so oversizing of the battery is unlikely, meaning that each cell will be pushed to supply as much power as the manufacturer allows. Uneven current sharing under these conditions may become problematic and can push cells beyond their limits. Research is necessary to determine if cells connected in parallel will share current evenly. Imbalance may potentially cause cells to prematurely fail within the pack due to excessive heat and cycling. Even if the cells do share current evenly at the beginning of their useful life, it is likely that they will age at an uneven rate due to differences in construction, materials, and location in the array caused by thermal effects. A cell with higher internal source impedance will discharge a portion of its useful energy as heat rather than to the load. The additional thermal load on the array may also contribute to the aggregate aging of the parallel array. When one considers that a modest pulsed power system can include hundreds, and possibly even thousands, of cells, the need to understand and accurately predict cell behavior is an economic and safety necessity.

In order to develop this understanding, research is being performed on $LiFePO_4$ cells with a 26650 form factor using a load profile identical to that utilized to charge a pulsed power device at NRL. The objective of this work is to carry out some experimentation on a sample of controlled cells to test the hypothesis that changes in a single-point impedance value can be correlated to cell aging when 26650 $LiFePO_4$ cells are cycled using a standard, non-abusive, pulsed discharge profile in both single-cell and parallel-cell configurations. Another hypothesis that will be tested involves the aging of cells as a function of cycle in a parallel array. The cells will age at an irregular rate, which will cause an uneven increase in equivalent series resistance (ESR), which in turn imbalances the parallel cell discharge and causes premature aging of the parallel group when compared to the lifetime of a single cell.

In support of that hypothesis, we may call on the work reported in Refs. 1, 2 on 18650 $LiCoO_2$ cells, which demonstrated that a single-point impedance diagnostic may be identified for assessing battery health. This work, however, aimed at overcharging, not cycling, the tested cells for damage analysis. Furthermore, it was carried out on $LiCoO_2$ cells, not the $LiFePO_4$ cells that we are interested in. Nevertheless, it appears that the proposed single-point impedance method is effective due to the sensitivity of the EIS diagnostic to the solid electrolyte interface (SEI) in the battery. A properly formed SEI layer on the surface of the negative and positive electrodes protects against continuous electrolyte decomposition of those surfaces.[3] In our experiment, the cells are cycled, particularly at high C rates; as a result, the SEI will degrade and the protection is diminished or negated entirely, leading various effects from capacity fade to power fade and potentially destructive dendrite growth.[4,5] The impedance associated

*Electrochemical Society Student Member.
**Electrochemical Society Member.
[z]E-mail: brett.huhman@nrl.navy.mil

with the SEI is in the 100–1000 Hz range of the electrochemical impedance spectrum for lithium batteries.[6–12] A C rate is defined as the rate at which a battery is discharged relative to its theoretical maximum capacity. For our work, 1 C = 2.6 AH.

It is worth reviewing related work that has been performed on parallel cells. For instance, Gong et al.[13] carried out experimentation on automotive lithium cells to investigate and model series-parallel arrays. Unlike our work, they studied cells that had been previously used so that each of them was at a different SoH with varying level of capacity fade on them. The results presented appear to confirm the hypothesis that when cells of varying impedance are mixed within a parallel connection of cells, there is significant variation in the current sourced by each that follows the SoH of the cells. Gogoana et al.[14] demonstrated that a 20% variation in the internal resistance of two identical cells connected in parallel can lead to a 40% reduction in cycle life, when compared to two cells of similar internal resistance connected in the same manner. The experiment consisted in cycling the cells at 4.5C; this is in contrast to our work where the cells are cycled at 10C. Higher C rates are of interest to us because it leads to higher heat generation, which in turn leads to premature cell degradation. At such rates, even small variation in current sharing may induce significant variation in the heat generation and further exacerbate uneven cell aging. Simulation results presented by Feng et al.[15] suggested the possibility of thermal runaway when asymmetry is developed between cells connected in parallel. Unfortunately, these results were not backed up by any measured data, and therefore were not conclusive. By contrast, in our NRL test all of the cells stand are instrumented and carefully monitored for excessive thermal excursions.

Correct interpretation of the data gathered from a parallel array can only be made if identical cells are analyzed individually first. This is precisely what we have done; specifically, we carried out a series of experiments to characterize individual 26650 $LiFePO_4$ cells. The impedance response as a function of state of charge (SoC) was measured and lifetime data was collected when they were cycled at 10C and 1C. While those experiments were being performed, a 4P1S array constructed of four identical lithium iron phosphate cells was constructed using a novel instrumented testbed. These cells were initially characterized and then data was collected to study the level of current imbalance and the impact it had on cell aging. Next, we will describe the experimental setup constructed and will analyze the data collected to date to test the validity of the aforementioned hypotheses.

Experimental

The experiment performed has two primary objectives: (i) evaluate current sharing and degradation within a parallel array of cells via the setup of a parallel cell testbed and (ii) characterize aging at different two different discharge rates by carrying out an individual cell lifetime study. The parallel cell array was being used to understand how a multi-parallel cell battery operates when it is populated with cells that have a known ESR measured from 10 kHz to 0.1 Hz, with a 10 mV perturbation amplitude. A programmable DC load was utilized to load the battery under representative profiles of interest. It should be noted that all of the experiments discussed here were performed within a thermal chamber set to maintain the ambient air at 25°C. The temperature maintenance was periodically verified using the history function of the controller, in addition to each cell having an independently monitored thermocouple.

A significant effort was expended to select which batteries would be used within the evaluation. An initial population of 180 cells, which were all newly obtained from the manufacturer, was cycled according to the procedure described in Refs. 16, 17. To ensure proper solid electrolyte interface (SEI) layer formulation, it was desirable to choose cells that had a 1C (2.6A for these cells) charge/discharge capacity variation of no more than 0.2%. From the cells that passed the initial capacity variation requirement, a second filter was applied using ESR. Cells were grouped into divisions of 0.1 mΩ at the 1 kHz frequency, and the largest group in a single division ±0.1 mΩ

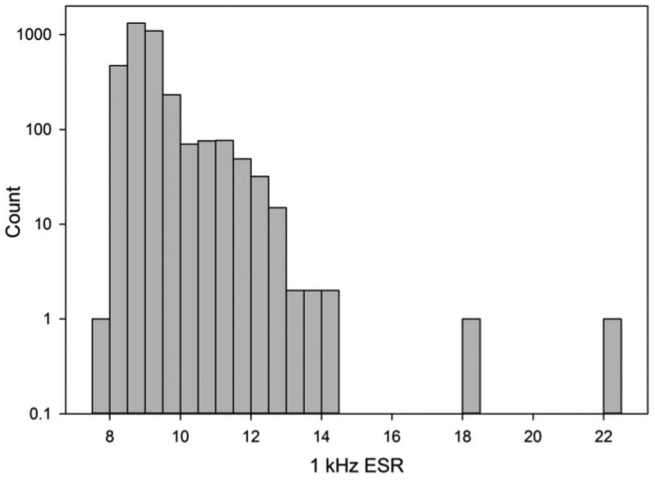

Figure 1. Frequency plot of the 1 kHz ESR values for 3,327 new cells from the battery manufacturer.

(equipment measurement variance) was selected for experimentation. Within this population of cells, the ESR was 9.3 mΩ. It is important to note that the cells selected from this smaller population for specific experiments were selected randomly, and represent multiple lots from the manufacturer over several years. One can therefore state that the subsequent data recorded can reasonably represent a typical cell from this manufacturer.

The variability in the cells received from this manufacturer is shown in Figure 1, where 3327 cells were measured as they were removed from the battery conditioning equipment at NRL to be installed for another project, of which some lots were included in our work. While the majority of the cells were between 8 and 9 mΩ, there was a significant number of cells that had 1 kHz ESR values as high as 22.4 mΩ. This variability demonstrates the need to perform post-manufacturer filtering before installation in an operational system to obtain a statistical homogeneous cell sample, an experimental design requirement for testing our hypothesis stated in the introduction.

Parallel cell testbed design.—A prototype discharge testbed was designed and built to collect the initial data from the 4P1S battery array. Lessons learned from the design of this array were applied to a second-generation testbed, shown in Figure 2. The testbed was improved significantly, with the replacement of the 10-gage Cu wire with blocks of ultra-conductive copper (Cu-101). The hall-effect current sensors were replaced with high-precision current viewing resistors

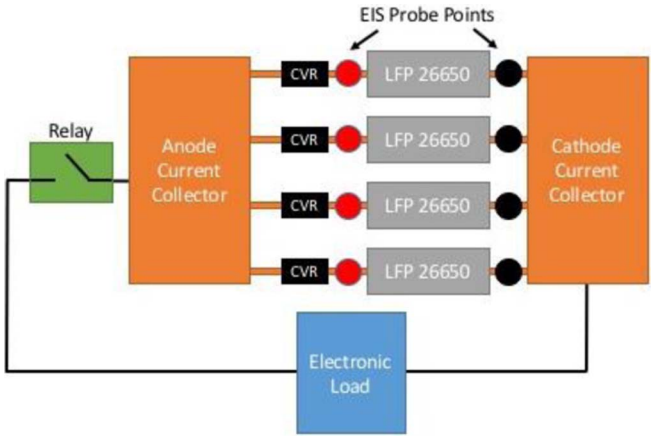

Figure 2. Schematic drawing of 4P1S battery array with connections to current sensors, electronic load and EIS probe points.

to improve current measurement accuracy. Additionally, banana plug sockets were installed to facilitate the insertion of EIS probes with highly-repeatable, low-impedance contacts to the individual cells. Each cell line had a section of Cu-101 between the current viewing resistor and the anode current collector that can be removed to isolate the battery from the group for impedance analysis. The relays and large gage wire connected to the electronic load remained the same for both setups.

The impedance between each cell and the testbed was a concern for this experiment. The original design used welded Cu-110 0.0762 mm shim stock for battery tabs. While the welds appeared to be stable, there was no consistency on the welds between each battery, which was believed to be a source of error in the experiment. The revised design utilized Ni-201, or commercially pure nickel. While its resistivity is much higher than copper, the use of custom 3-D printed battery holders and standardized spot welding practices ensures conformity across the cells.

The system was discharged into a programmable electronic load manufactured by Kepco Inc. and recharged with an HP 6554A DC power supply. The National Instruments LabVIEW programming language was used with the IEEE-488 protocol to program the load and the source devices during the experiment. The current viewing resistor data was amplified by means of Dataforth SCM5B30-02D analog voltage modules, and the voltage of each cell was individually monitored by means of a differential voltage measurement device. The final set of instrumentation used in the experiment was thermocouples. Each cell in the array had three Type-T thermocouples attached at three different locations, namely in the middle of the case, on the anode tab, and on the cathode tab, respectively.

Lifetime performance study.—Two sets of cells were used to evaluate the long-timescale lifetime performance of the types of cells used in the parallel array. Each set was comprised of eight cells chosen at random from the sample set described earlier. Both sets were selected for evaluation under pulse discharge conditions at a 1C rate (2.6A) and 10C rate (26A), respectively. The pulsed discharge procedure consists of carrying out cycles of a discharge of 4 seconds followed by a rest of 2 seconds for duration of 5 minutes. At the 1C rate, this resulted in 0.0029 Ah being extracted from each cell at roughly 0.116% depth of discharge. At the 10C, rate, 1.44 Ah is extracted at 57.6% depth of discharge. While these discharges appear to be relatively shallow, they are intended to be representative of a real system under test.

A MACCOR Series 4000 computerized battery analyzer was used to cycle the cells under lifetime test. Each cell was assigned an independent channel for analysis and was continuously charged and discharged for a set number of cycles. Temperature, current, and voltage were logged to a file for later analysis if necessary. To eliminate individual channels as sources of error, the channels assigned to specific cells were rotated so that any error in the machine would be evenly distributed in the population.

At the end of each rotation, each cell had an EIS sweep performed from 10 kHz to 0.1 Hz, with a 10 mV perturbation amplitude using a Solartron Analytical ModuLab XM system. The 1C population was set on a 200-cycle rotation, as the depth of discharge was very shallow and many cycles were expected to be necessary to show any aging of the batteries. Conversely, the 10C population was on a 25-cycle rotation to increase the resolution of EIS scans due to the expected accelerated damage on the cells at the higher discharge rate. EIS analysis was also performed on the parallel cell array. Due to the low ESR of the cells under test (≈9mΩ), the instrumentation was switched from potentiostatic to galvanostatic mode, with a 200 mA perturbation. EIS sweeps were performed on a 50-cycle basis for the parallel array, with an aggregate spectra and individual cell sweeps each interrogation interval.

State of charge measurements.—Seventeen separate cells from the experimental group, that were not actively used in any other experiment, were charged from 0% SoC to 100% SoC in 10% SoC increments. The cell was discharged to 2.0 V at a rate of 0.1 C in multiple steps with rest periods to allow recovery before resuming discharge. Once the cell exhausted its electric energy, two EIS cycles separated by a 5 minute rest period were performed with a frequency range of 10 kHz–0.1 Hz for each step beginning at 0% SoC. A rest period of 30 minutes was used after each 10% charge increment before the EIS cycles was started. The cell was charged at 0.1C to minimize internal heating during the recharge process. Each cell was measured individually, while the probes were not moved between experiments to maintain a consistent contact resistance. The entire cycle was automated by the ModuLab software.

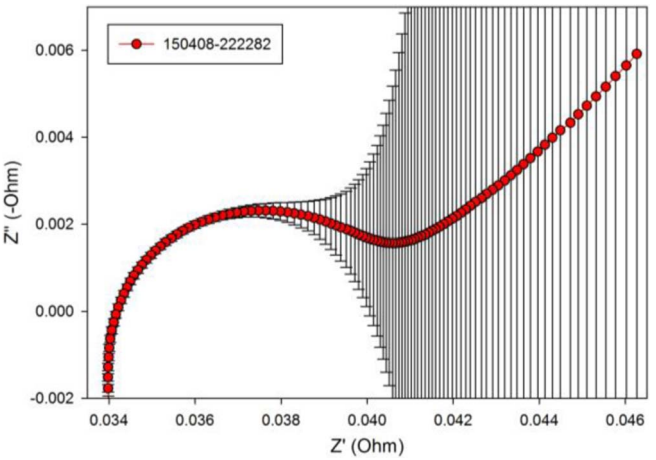

Figure 3. Nyquist plot with standard deviation error bars of a single cell as the SoC is varied from 0% to 100%.

Results and Discussion

An understanding of the baseline behavior of the parallel cell array is necessary before any valuable conclusions can be drawn. Data from the three sets of parallel experiments were collected and are discussed here. It is noteworthy to mention the importance for the collected single-cell data to be analyzed first before applying them to a parallel cell array, because the resulting data cannot be interpreted otherwise. Indeed, the lifetime data collected from a single cell with the specified discharge profile is essential to determine the expected drift in ESR as a function of C-rate and cycles, which will be used with the parallel cell array to simulate the aging process of the latter. In conjunction with the lifetime data is the expected SoH frequency, which will be the primary diagnostic when examining the SoH of a parallel array of cells.

Determination of the SoH frequency.—Lithium-ion cells have a unique impedance response that changes with its state of charge (SoC). Seventeen cells from the lot discussed earlier, were baselined and placed on a test fixture to record their EIS as a function of SoC. This part of the experiment was meant to identify the singular frequency which has the least amount of deviation in both real and imaginary impedance. As previous studies have concluded, this frequency can be used as a reliable SOH metric even as the cells lose reversible capacity over their lifetime.[1,2,18,19] Example data collected from one of the seventeen cells is presented in Figure 3, with the error bars indicating one standard deviation from the median values of the data. It appears the first half of the semi-circle in the high frequency region has relatively low variations in the data, and after this point (approximately 100 Hz), the data begins to vary significantly. Standard deviation is an appropriate descriptive statistic for this application, as analysis of the data in the region of interest (100–1000 Hz) shows that the median deviates from the mean no more than 0.4 mΩ for both the real and imaginary data, indicating that for each frequency and SoC combination the distribution is nearly symmetric. Furthermore, it is found to be approximately normal for the specified frequency range.

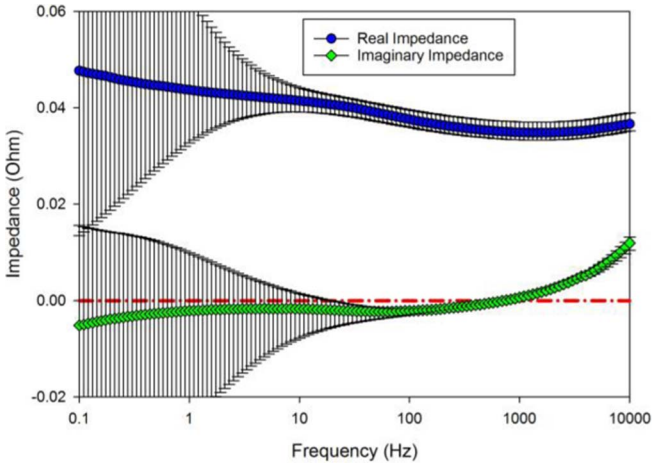

Figure 4. Median values of the real and imaginary impedance data along with the associated standard deviations shown by error bars.

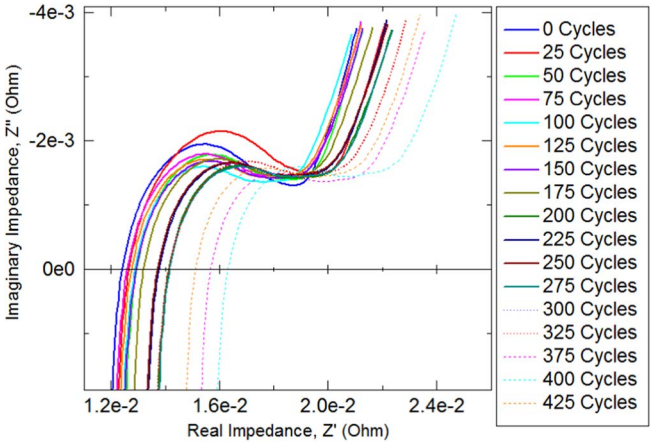

Figure 6. EIS spectra for single cell lifetime testing with pulsed load profile.

The data collected from the seventeen cells can be compiled into a single graph to demonstrate the trends. As shown in Figure 4, the imaginary impedance median values along with the associated points situated at one standard deviation away from them are negative from approximately 35 Hz to 600 Hz. Note that a positive value for the imaginary impedance suggests inductance effects, which are not of interest here. Furthermore, we notice that the standard deviations of the real impedance values barely change from 10 Hz through 10 kHz over all of the various SoC. However, for both the real and imaginary impedances, it is expected that their values will exhibit large variation as the frequency decreases because the processes associated with lower frequencies are more sensitive to the SoC of the cell.

Further examination of the plots displayed in Figure 5A, which are those of the median values of the standard deviations shown in Figure 4 versus the frequency, reveals that the standard deviation of the real impedance flattens out starting from 100 Hz, while the imaginary impedance continues to decrease. A zoom in of the standard deviation data is shown in Figure 5B, where the frequency range was limited to 100–250 Hz. As shown, the median values of the real impedance along with their associated standard deviations of error are equal for two specific frequencies, namely 145 Hz and 158 Hz. We may expand the frequency range of interest to 174 and 191 Hz, but the one-standard-deviation error bars maintains a plateau only between 145 and 158 Hz, with a negative slope starting 209 Hz. In this same frequency band, the median value of the imaginary impedance's standard deviation is approximately 0.4 mΩ, which is a very small deviation from the median values on all seventeen cells for the entire 0–100% SoC regime. Because of the constant characteristic of the standard deviation of the real impedance values and the overall low standard deviation of the imaginary impedance values around 158 Hz, the latter frequency was selected as the frequency of interest for SoH determination, f_{SoH}. This means that only analyzing how the impedance varies at 158 Hz may be sufficient for revealing how the cell ages as a function of its cycle life.

Cell lifetime data with EIS.—Cell performance as a function of cycle life when they were cycled using a pulsed discharge procedure at two different C-rates, namely 1C and 10C, will be presented next. The EIS spectra were recorded at regular intervals at 10C rate (25 cycles) and 20C rate (200 cyles), with the former used more frequently than the latter. A plot of the Nyquist data for a single cell at the 10C rate is displayed in Figure 6. Due to experimental equipment limitations, the probes were removed repeatedly during the experiment, which resulted in some variability of the real resistance. The median value of this cells real resistance amounts to 13.6 mΩ with a standard deviation of 1.12 mΩ. The baseline and 25-cycle sweeps were not given much weight since it is very likely that the electrochemistry was still settling over the time span of the experiment. Interestingly, it is observed from Figure 6 that the spectra for cycles 375–425 correspond to a move of the real impedance to the right; we do not have an explanation for

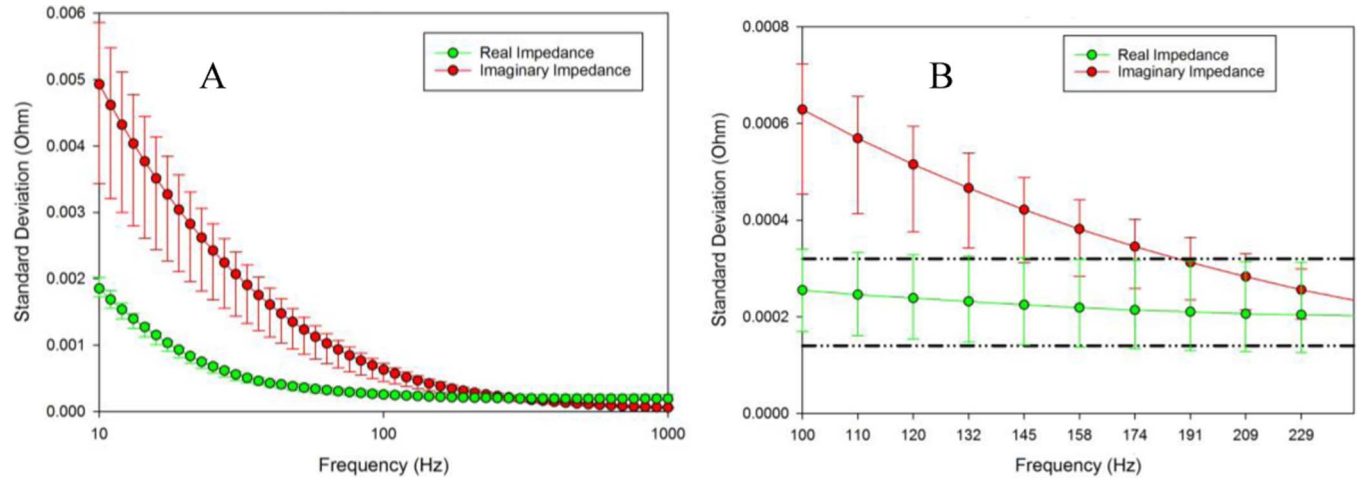

Figure 5. Distributions of real and imaginary impedance standard deviation median values as a function of frequency, where A) is from 10–1000 Hz and B) is from 100–240 Hz.

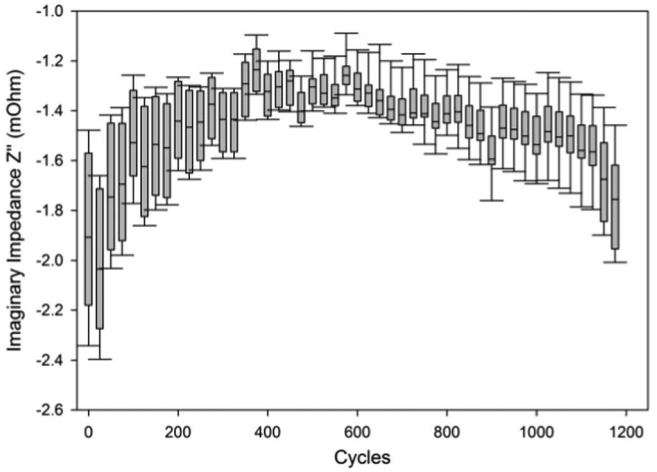

Figure 7. Imaginary impedance at 158 Hz as a function of cycle number for eight cells subject to lifetime testing at 10C. End of life reached at 1175 cycles.

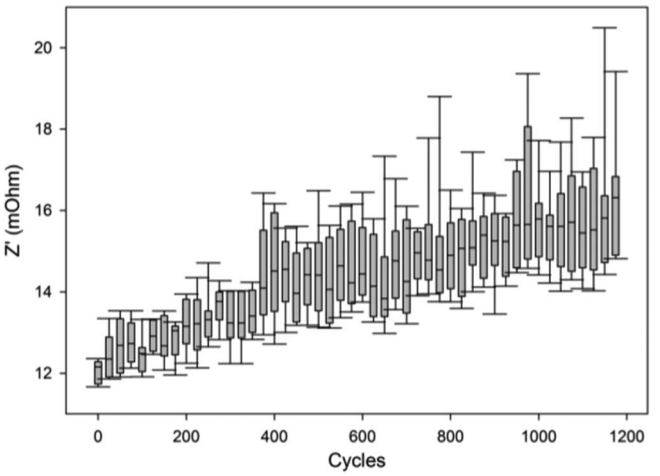

Figure 9. Real impedance as a function of cycle at 1 kHz for cells cycled at 10C. The data indicate a progression toward a higher real impedance with cycle aging.

that phenomenon, although it can be speculated that it is related to the aging of the cell. It is difficult to determine specifically the cause of any changes in the real resistance in this experiment. A repeated experiment with permanently attached probes would be required to eliminate the probes as a source of error.

Using the SOH frequency identified in the earlier section, a box plot of the imaginary impedance at this frequency as a function of cycle number was generated and displayed in Figure 7. As observed, at low cycle numbers, the interquartile ranges of the imaginary impedance values are rather large. However, as the cells are repeatedly cycled, they narrow down around a median value of 1.3 mΩ. The interquartile range begins to decrease from 50 cycles until about 200 cycles. A particularly interesting aspect of this diagnostic is that it focuses only on the imaginary impedance while minimizing the effect of the real impedance, as contact resistance errors are introduced with the repeated insertion and removal of the instrument probes.

A plot of the imaginary impedance at 158 Hz as a function of cycle number measured from the cells in the 1C lifetime testing group is displayed in Figure 8. Albeit at a slower rate, the 1C cell group converges to a single frequency as does the 10C group. The most interesting feature seen is that only after 200 cycles do the cells begin to exhibit some small variability between cycles. This may be of importance during the construction of a parallel cell pack, as it may take many more cycles than previously believed to settle the electrochemistry.

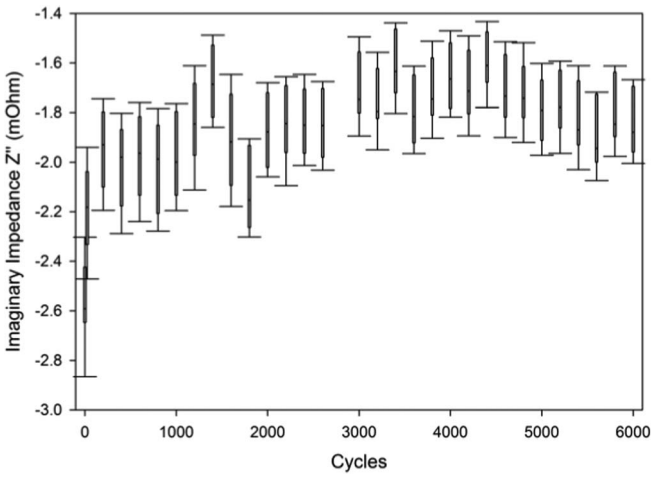

Figure 8. Imaginary impedance at 158 Hz as a function of cycle number for eight cells subject to lifetime testing at 1C.

As shown in Figure 9, the median ESR at 1 kHz is approximately 12 mΩ at the beginning of the cycling process. After 625 cycles, the median value increases to 14 mΩ with a 1 mΩ standard deviation. This data supports the hypothesis that the cells will age unevenly and presents a range of possible ESR values after 450 cycles of usage. We may speculate that a large portion of the variability between readings is due to resistive contacts with the EIS probes changing between data measurements. A follow-up study with permanently attached EIS probes and multiple data channels would allow for precision determination of the ESR growth as a function of cycle. However, it is believed that with a sufficiently large sample size such as in our work, the data recorded are sufficient to describe a typical cell response as a function of cycle and C rate.

The convergence of the imaginary and real impedance values in the paralleled cells can be explained by the stabilization of the SEI film in each one. Cells which have a higher impedance initially most likely have a more developed SEI film on the surface of the graphite anode. This means that less bare electrode is exposed to the electrolyte solution initially in these cells. Therefore, the impedance will also increase at a slower rate in these cells. On the other hand, the cell with a lower impedance have less developed films and a greater amount of bare electrode exposed. Thus the potential for impedance increase is higher in these cells initially. As the electrodes in all the cells reach a stable state in SEI development, their impedances equalize and the cells begin to contribute an equal amount of current in the parallel configuration.

Parallel array discharge data results.—From the EIS spectra measured from the seventeen cells, data collected at 50% SoC was examined to identify four cells with nearly identical Nyquist plots. As shown in Figure 10, four cells were identified that met the selection criteria, with a real axis crossing median of 13.073 mΩ and a standard deviation of 41.42 μΩ. Each of the four cells was placed in a similar cell holder, and the EIS probes were semi-permanently attached. Each cell was discharged to 0% SoC and recharged in 10% increments with a programmed 30 minute pause prior to an EIS sweep to allow the electrochemistry to settle and equilibrate the internal cell temperature. After the cells were installed in the testbed, a high-precision 1-kHz milliohmmeter was used to determine the resistance from the battery anode to the collector plate for each cell. A median resistance of 3.288 mΩ with a standard deviation of 0.121 mΩ was recorded. This resistance value was determined to be sufficiently low for the cells, given their 9.3 mΩ 1 kHz source impedance with the ESR meter.

The array was programmed to provide a current of 104 A into the electronic load (EL) over a 300 second period, with 50 pulses of four seconds on, two seconds off. Based on the 1-kHz ESR impedance

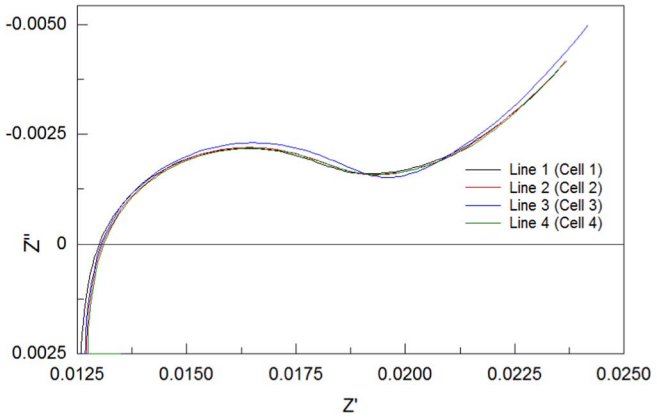

Figure 10. Cells selected for baseline analysis in parallel cell array. Data was recorded in situ for each cell (isolated from the group) at 50% SoC in the array.

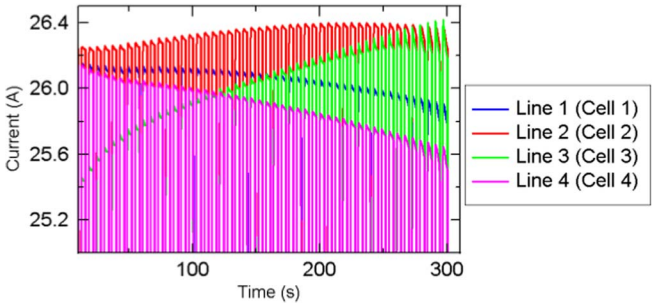

Figure 11. Current recorded from parallel array at 10C with pulsed discharge program on the EL.

match of 9.2 mΩ (±0.1 mΩ instrument error) and the full-spectrum EIS close overlay, the expected response of the array would be to have close match of current discharge with slightly less current from Cell 3 to track with the slightly higher impedance and lower frequencies. This is somewhat reflected in the data shown in Figure 11. As observed, there is a 3% difference between the peak discharge current of 26.4 A on Cell 2 and the lowest current output from Cell 4 at 25.6 A. The low overall cell-to-cell variation tracks well with the effort to balance the discharge lines and force any changes to the battery cells. As explained earlier, the current changes over the time of the pulsed discharge test can be explained by the SEI film development. Cell 2 appears to source current at a relatively steady rate, while Cell 4 is decreasing as Cell 3 increases. The slight decrease in Cell 1 appears to track with the slight increase in Cell 2. This phenomenon has been clearly illustrated in these parallel experiments and should be researched further in future efforts to determine its effect on long-term degradation and power quality in a larger system.

The voltage recorded for each cell is displayed in Figure 12. Cell 1 has the lowest voltage, which indicates that it is under stress sourcing

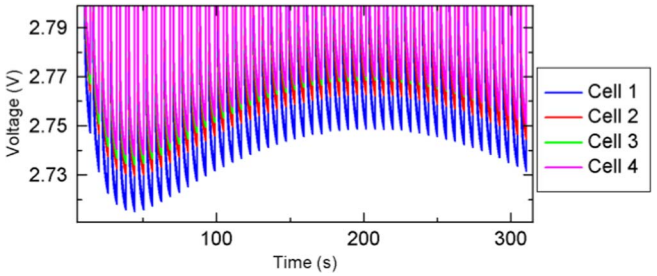

Figure 12. Voltage recorded from the parallel array at 10C with pulsed discharge program on the EL.

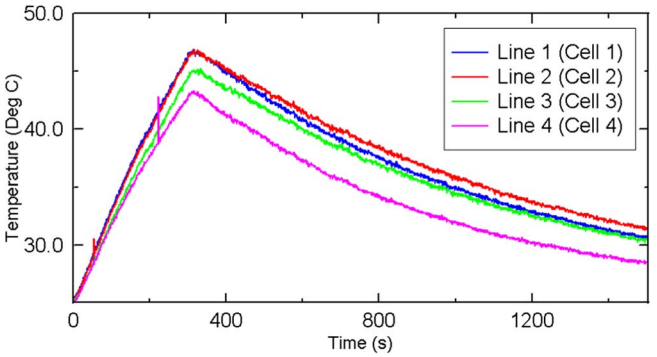

Figure 13. Cell case temperatures from the parallel array at 10C with pulsed discharge program on the EL.

current. Cells 3 and 4 have overlapping voltages under load, and Cell 2 is between the two extremes. One can observe the load voltage increasing at approximately 50 seconds, which corresponds to the temperature data reaching 28°C. Given that the cells have an initial temperature of 25°C, a measurable temperature rise on the case of each cell indicates sufficient internal heat is being generated to reach the exterior case and cause the internal ESR of each cell to decrease.

A plot of the cell case temperatures for the entire discharge cycle and recovery period is shown in Figure 13. Cell 4 has the lowest overall temperature, which is expected since it sources the least amount of current. Temperatures variation is a result of imbalance in the current delivered by each respective cell to the load, shown earlier in Figure 11.

The data shown in Figures 10–13 describe the initial state of the parallel array, which appears to support the hypothesis that four cells with nearly identical Nyquist EIS plots would share current evenly. However, as shown in Figure 14, after 100 cycles the Nyquist plots have started to diverge and the cells no longer have identical impedance responses. In Figure 15 the EIS spectra is shown for every 200 cycles from 0–600 cycles, and the trend is observed to continue with the impedance response different for each cell. After 200 cycles, the diffusion region for all of the cells is nearly identical, with approximately the same slope. After 400 cycles, however, Cell 2 has a distinctly different slope in the diffusion region. This does not appear to affect discharge performance, and may just be a symptom of aging in the cell. The overall shape in the charge transfer kinetics region appears to be the same for all of the cells for the 600 cycles recorded.

A plot of the aggregate EIS spectra is shown in Figure 16. This data was normalized to zero for ease of comparison, as the real impedance changed significantly over time as the probes were repeatedly inserted and removed. In general, the diffusion region appears to be relatively similar across all of the cycles sampled, with no deflections to the right or left of the main body of data. The charge transfer kinetic regions for the first 350 cycles also have approximately the same shape, indicating relatively healthy SEI layers for the cells. At the 400 cycle mark, a depression begins to appear in the semicircle region. It appears a change in the fundamental time constant for this region is occurring, with a progressive decrease in the peak value of the semicircle. It is likely the SEI layers are starting to show signs of aging.

A plot of the total energy delivered to the electronic load per cell as a function of cycle is shown in Figure 17. For the first nearly 150 cycles, all of the cells appear to source approximately the same amount of energy, with some various cycle-to-cycle. In this period, Cell 2 appears to dominate a portion with the most energy sourced. After about 150 cycles, Cells 2 and 3 source the most energy with the other two cells at about the same. At the 200 cycle mark, however, Cell 3 is suddenly sourcing ≈200 J more than Cell 2. This trend continues, with Cell 3 reaching a peak of 6% higher energy than the other three cells before a slow decline to 4% as the cells begin to age with the onset of power fade.

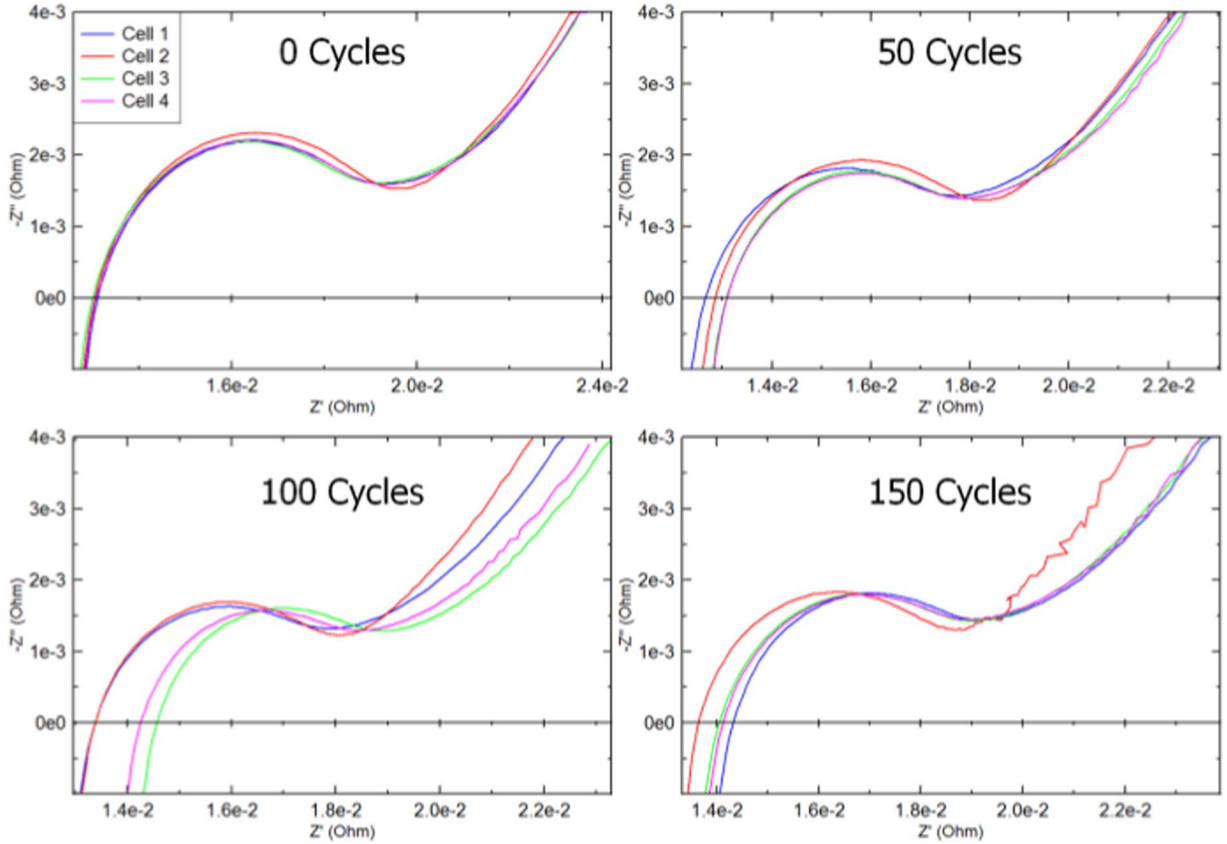

Figure 14. Individual EIS spectra for the four cells in the parallel array as a function of cycle for the first 150 cycles at 50% SOC.

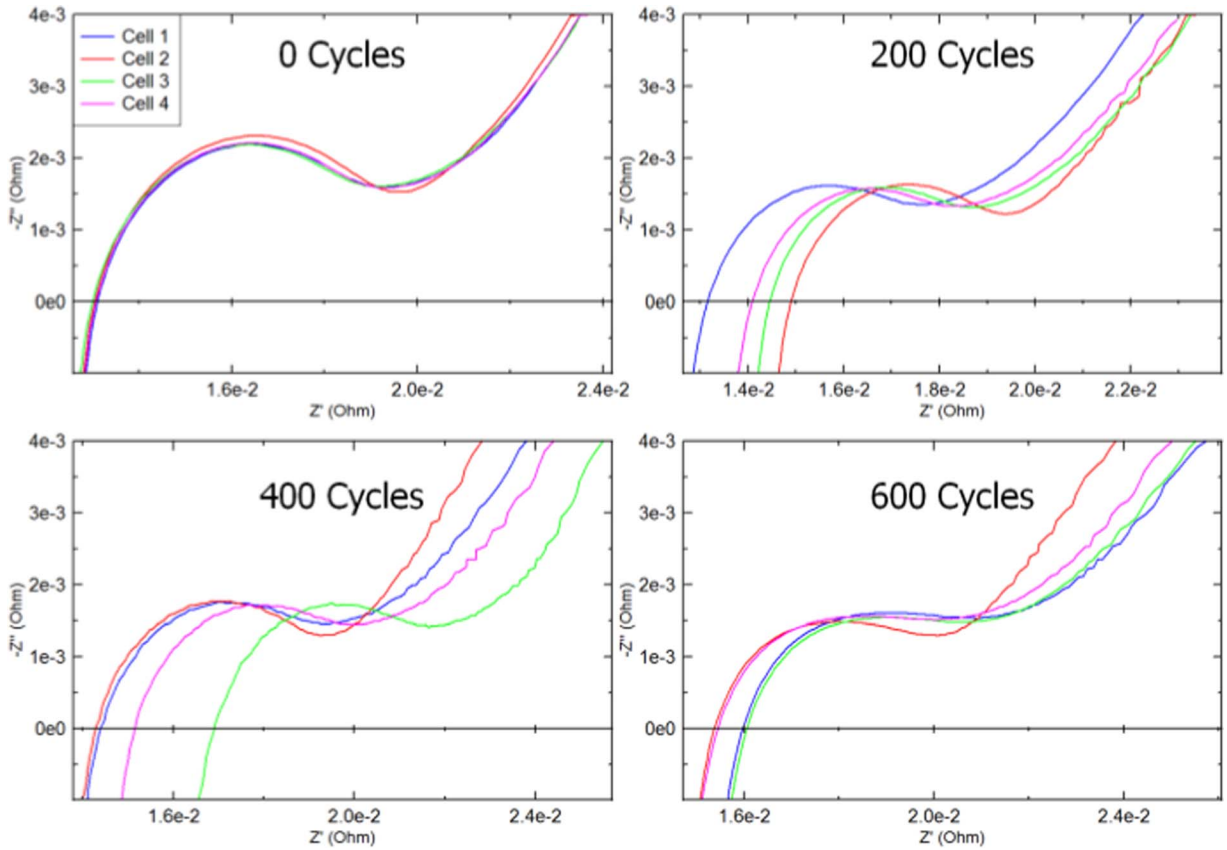

Figure 15. Individual EIS spectra for the four cells in the parallel array as a function of cycle at 50% SOC.

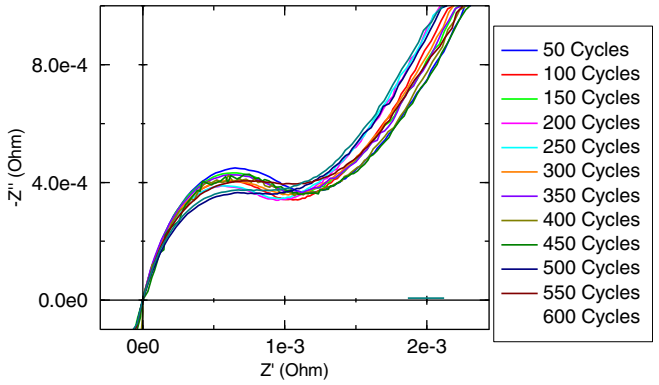

Figure 16. Normalized aggregate EIS spectra for the four cells in the parallel array as a function of cycle at 50% SOC.

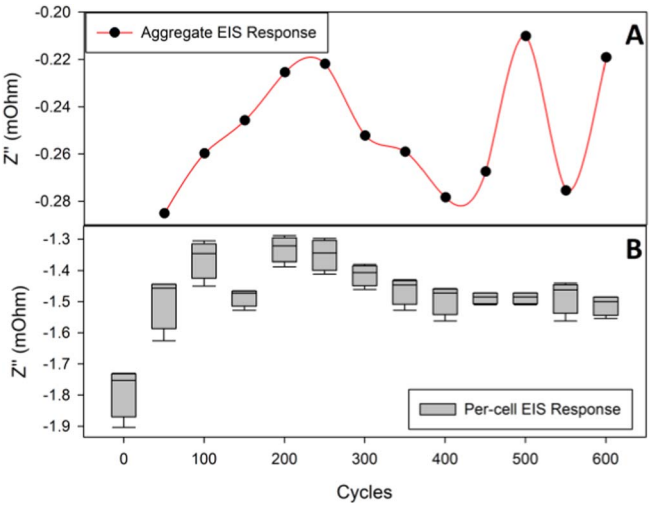

Figure 18. Imaginary impedance response at 158 Hz as a function of cycle for all four cells in the parallel discharge array, with aggregate response (A), and individual cell statistics (B).

Based on the single-cell data shown in Figure 18, it appears the aging of the SEI layer is being artificially accelerated by placing the cells in a parallel array. The imaginary impedance at 158 Hz follows the initial progression shown in Figure 7, with −1.9 mΩ (median) at 0 cycles and −1.35 mΩ (median) at 100 cycles. The divergence occurs at 450 cycles on the parallel data, with an imaginary impedance of −1.35 mΩ. The drop to this value does not occur on the single cell data until at the earliest 775 cycles (single cell) and 900 cycles (median value). Since the controllable conditions are the same for both tests (pulse discharge rate, recharge rate, environment), one must conclude that the changes observed in the 158 Hz response must be related to changes in the SEI layer.

The aggregate EIS data shown in Figure 18 follows the general trend of the single-cell data until Cycle 450, where the imaginary response for the array as a whole begins to oscillate. Under initial examination when compared to the flat response shown in the single-cell data for Cycles 450–600, it is unclear why the response with all of the cells in parallel has a sudden periodic quality as a function of cycle. However, if one looks at Figure 17, there is a sudden drop in the energy delivered to the load for all of the cells at the 450 cycles mark. It is possible that the four cell impedances in parallel have lowered the effective impedance to a point such that other effects in the batteries may suddenly dominate the response. Temperature effects are believed to be negligible, as the array was discharged and interrogated in a thermal chamber held at 25°C. For this data, the array was allowed to equilibrate to the ambient temperature for at least twelve hours prior to the recording of the EIS spectra. Each cell had three thermocouples attached to the casing, and the chamber temperature was periodically verified with a history plot on the chamber controller. If this data is repeatable for other arrays, it appears the EIS single-frequency health diagnostic may be more sensitive to battery SOH in the parallel-cell mode than in the single-cell mode. In this case, it appears the power fade aging phenomenon was detected.

Parallel array EIS modeling.—An equivalent circuit model of the EIS spectra for the batteries used in the parallel array was created, and is shown in Figure 19. Each simulation had a Chi-squared value of less than 1E-5 to ensure a close fit. The model uses an inductor in parallel with a resistor to model high frequency effects, such as the inductance associated with probe cables and internal battery connections. A series resistor was included to model the contact resistance, and at this time is lumped with the series resistance associated with the electrolyte solution. Since the probes were continuously removed between each sampling event, it is difficult to determine precisely the difference between changes in the electrolyte and the contact resistance of the EIS probes. Two series ZARC elements follow Rs, with the first one modeling the SEI layer and the second capturing anode effects. Finally, a Warburg open impedance model is used to match the cathode diffusion. A comparison between the measured spectra and the model

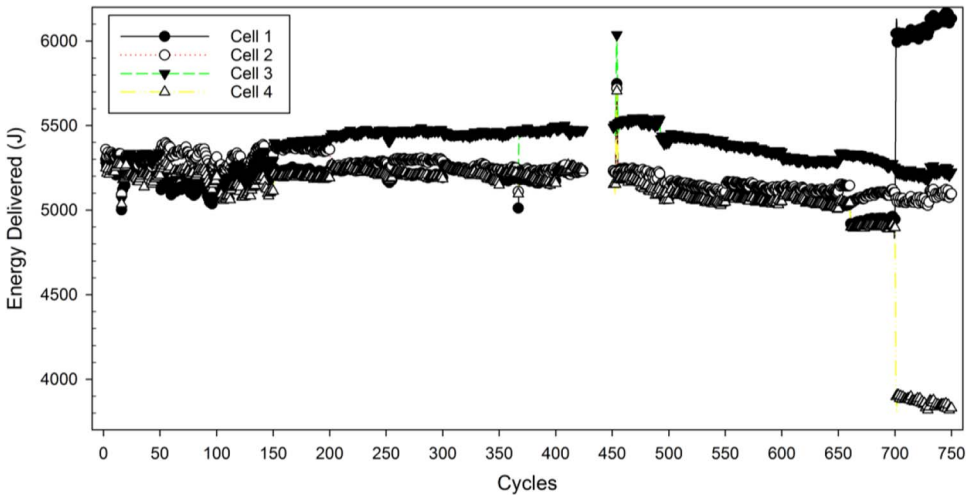

Figure 17. Energy delivered to the electronic load per cycle per cell in the parallel array. End of life reached at 750 cycles.

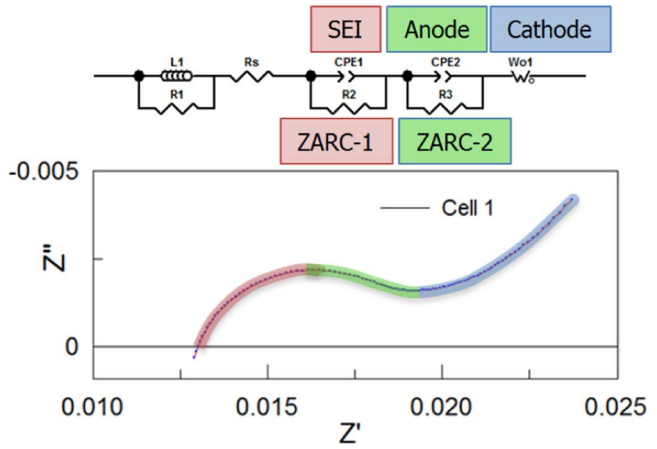

Figure 19. Electrical circuit model for EIS spectra.

fit is shown in Figure 20, and the initial simulation values are shown in Table I.

The standard deviations for each of the model elements for each cell in the parallel array are shown in Table II. The inductance element L1 appears to be relatively stable, with σ in the 10–7 range. The low change in L1 would indicate that the change in inductance from the probe cables is negligible, as they were moved frequently between data acquisitions, and the cell components remained the same throughout the experiment. The resistor R1 had a higher σ than L1, and may be more sensitive to variations in the probe contacts. It is more likely there are high frequency effects outside the scope of this paper. The lumped series resistance Rs had a lower σ than expected, in the range of 10^{-4}. Given that R1 varies substantially more than Rs, it indicates that Rs may represent the solution resistance more than initially believed. The Warburg model appears to change little, with standard deviations for the Wo1-R and Wo1-T variables in the 10^{-7} range, and Wo1-P in the 10^{-1} range. This is likely due to the cells always returning to 50% SOC before a spectra is recorded, and also indicates that the cathode is experiencing relatively minor damage from cycling and calendar aging.

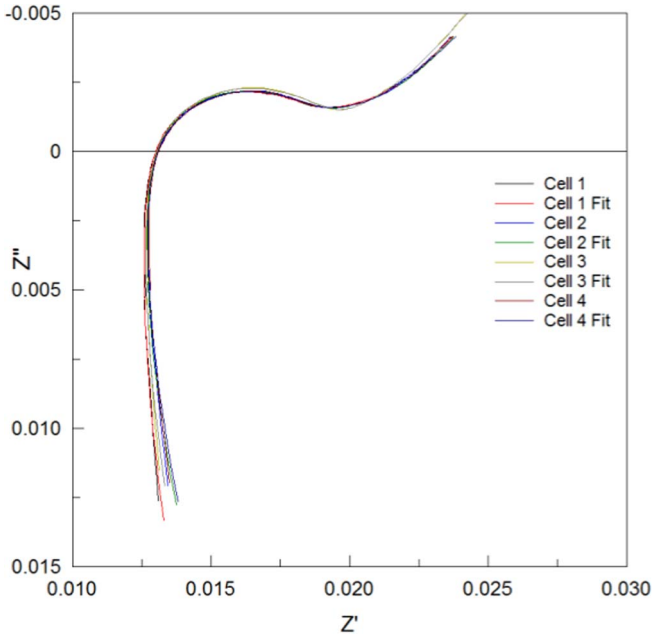

Figure 20. Measured EIS spectra for cells in parallel array with fitted data from EIS circuit model

Table I. Cycle 0 EIS Simulation Values.

Parameter	Cell 1	Cell 2	Cell 3	Cell 4
L1 (H)	2.09E-07	2.01E-07	1.91E-07	2.08E-07
R1 (Ω)	2.51E-01	1.64E-01	2.20E-01	1.19E-01
Rs (Ω)	1.23E-02	1.24E-02	1.24E-02	1.23E-02
CPE1-T (s)	1.82E+00	1.75E+00	1.68E+00	2.27E+00
CPE1-P	7.21E-01	7.26E-01	7.18E-01	6.80E-01
R2 (Ω)	6.38E-03	6.39E-03	7.01E-03	6.95E-03
CPE2-T (s)	1.16E+02	1.15E+02	1.89E+02	1.98E+02
CPE2-P	6.51E-01	6.18E-01	6.27E-01	9.44E-01
R3 (Ω)	2.15E-03	2.62E-03	2.58E-03	6.13E-04
Wo1-R (Ω)	3.04E-07	1.11E-07	1.02E-07	3.37E-07
Wo1-T (s)	6.50E-08	5.46E-08	6.89E-08	5.47E-09
Wo1-P	2.85E-01	3.09E-01	3.20E-01	2.50E-01

Table II. EIS Simulation Value Standard Deviations.

Parameter	Cell 1	Cell 2	Cell 3	Cell 4
L1	1.62E-08	1.60E-08	1.22E-08	1.78E-08
R1	3.98E-01	1.53E-01	2.83E-01	1.04E-01
Rs	6.75E-04	9.99E-04	6.89E-04	8.31E-04
CPE1-T	7.37E-01	7.11E-01	5.83E-01	6.67E-01
CPE1-P	6.80E-02	5.63E-02	1.17E-01	5.18E-02
R2	1.32E-03	1.25E-03	2.22E-03	1.33E-03
CPE2-T	4.39E+01	4.71E+01	1.44E+02	6.91E+01
CPE2-P	1.45E-01	1.55E-01	1.23E-01	2.18E-01
R3	1.43E-03	7.17E-01	6.90E-01	6.12E-01
Wo1-R	2.34E-07	1.56E-07	3.86E-07	3.83E-07
Wo1-T	1.11E-07	4.89E-08	9.40E-08	5.80E-07
Wo1-P	2.59E-02	1.70E-01	2.69E-01	1.49E-01

The two ZARC elements had the largest changes in standard deviation, and are therefore the most likely elements to examine for correlation between the measured electrical data and cell electrochemical state. The first ZARC element corresponds to the frequencies from approximately 750 Hz to 30 Hz, and can describe the behavior of the SEI layer.[12,20] As shown in Figure 21, the time constant for ZARC-1 changes significantly between Cycle 0 and Cycle 50, indicating the growth of the SEI layer as the battery is cycled. From Cycles 50–500, the time constant is approximately flat for all four cells. At 550 cycles, however, Cell 3 has a sudden drop in the time constant. When compared to the energy delivered per cell shown in Figure 17, this corresponds directly to a minor increase in energy delivered from Cell 3 while the other cells remain relatively constant. At the same time, the

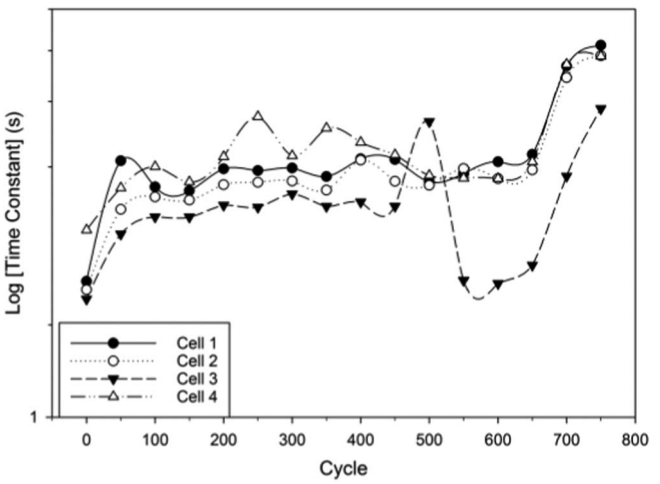

Figure 21. Time constant as a function of cycle for the ZARC-1 element in the equivalent circuit model.

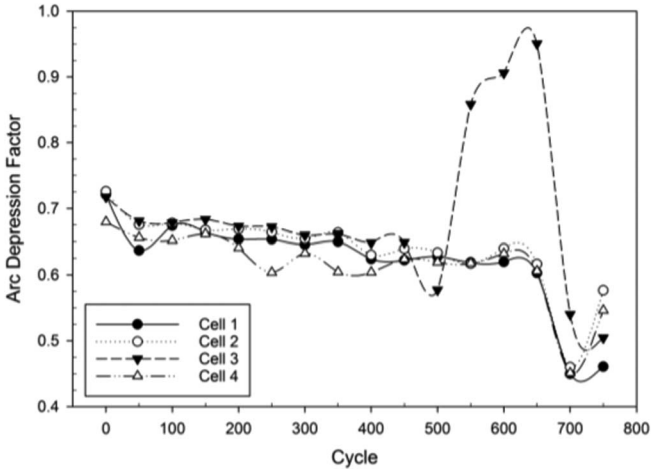

Figure 22. Arc depression factor as a function of cycle for the ZARC-1 element in the equivalent circuit model.

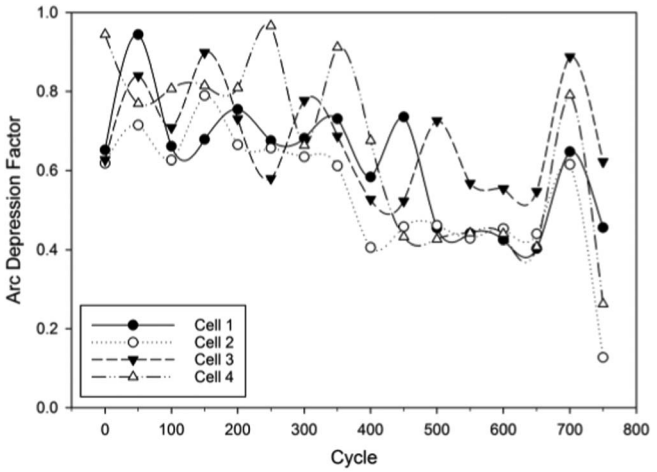

Figure 24. Arc depression factor as a function of cycle for the ZARC-2 element in the equivalent circuit model.

arc depression factor (CPE-P) for Cell 3, shown in Figure 22, changes from approximately 0.6 for Cell 3 at Cycle 500 to nearly 0.9 at Cycle 550. Growth in the time constant starting at Cycle 650 corresponds to the sudden power fade observed in Figure 17, and is possible that the SEI layer is increasing in size and inhibiting the Li+ ion charge transfer process. A uniform decrease in the arc depression factor at Cycle 700 also correlates to measured changes in the energy delivered per cell.

The second element corresponds to anode-specific mechanisms. As shown in Figure 23, the time constant is relatively flat until Cycle 500, which is to be expected for a properly conditioned new cell. After Cycle 500, the time constant for Cells 1, 2, and 4 decrease while Cell 3 increases slightly. This corresponds to the data shown in Figure 17, where Cell 3 increases energy output while the other three cells have lower total energy output. As the cycle number increases, the time constants continue to follow the trend shown in Figure 17, with a final value at end of life reflecting the observed collimation of the energy output from all four cells. The arc depression factor shown in Figure 24 oscillates between 0.6 and nearly 1.0 for all four cells until Cycle 500, where Cells 1, 2, and 4 are flat at approximately 0.5 until Cycle 650. Cycle 500 is the first cycle on Figure 17 where power fade is noticeable, and the energy slope of all four cells is decreasing as a function of cycle. This would indicate the observed power fade is affected by changes in the anode material.

Finally, the impedance data suggests that Cell 3 is suspect while the energy data presented in Figure 17 appears to show that Cell 3 is actually performing well compared to the other cells in the array. However, examination of the data shown in Figure 25 shows that Cell 3 is, in fact, suffering from capacity fade after approximately 300 cycles. The data in Figure 25 is the measured current from each cell during the final rest period of the pulse discharge, when the electronic load is disabled. In an ideal battery array, there should be very little current moving between cells as they are all balanced and at the same potential. The data recorded for this array, however, indicate that a recharge event is occurring on Cell 3 from approximately Cycle 250 through the end of life. Cells 1 and 2 appear to source the current that is recharging Cell 3 until Cycle 300, when Cell 2 provides most of the energy to recharge Cell 3. An inflection point is observed at Cycle 300 for Cell 3, as the slope of the current as a function of cycle changes suddenly and the energy to recharge the cell during the rest period continues to increase. Until Cycle 650, Cell 4 remains at a constant level sourcing comparatively little current compared to Cell 1 and Cell 2. This suggests higher source impedance for Cell 4, which is supported by the time constant data for the SEI layer shown in Figure 21.

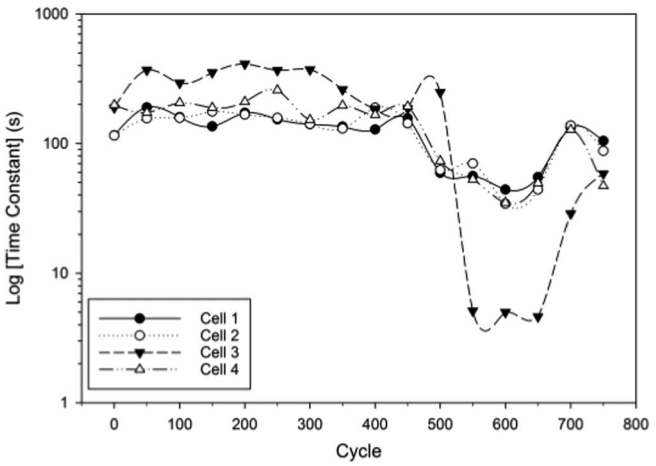

Figure 23. Time constant as a function of cycle for the ZARC-2 element in the equivalent circuit model.

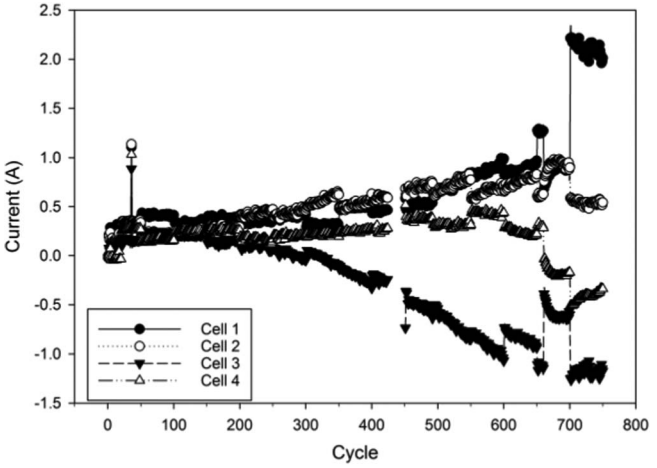

Figure 25. Current per cell as a function of cycle on final rest period in pulse discharge (296 s).

Summary

The US Naval Research Laboratory has initiated a series of experiments to evaluate the performance of a 4P1S battery array using electrochemical impedance spectroscopy to identify key frequencies that may describe battery state of health at any state of charge. Using a large sample number of cells, the state of health frequency, f_{SOH}, for these $LiFePO_4$ 26650 cells is found to be 158 Hz. When the f_{SOH} is examined for a set of four cells discharged in parallel, the individual EIS response for each cell shows an accelerated rate of aging versus data from baseline batteries. The aggregate imaginary impedance at 158 Hz for all four cells in parallel appears to be very sensitive to battery SOH, with a sudden change to an oscillation pattern that correlates to a drop in energy delivered per cell to the load. For this experiment, it appears to have detected power fade in the parallel array. An electrical circuit model was created for the parallel array, and the model appears to validate the observed changes in the energy delivered per cell. Cycle 500 appears to be a critical point, where the growth in the SEI layer begins to impede Li+ ion transfer. Changes in the anode also appear to affect the energy deliver per cell after Cycle 500, but a physical post-mortem analysis is required tie the changes to a specific mechanism.

A number of cells completed lifetime testing at the 10C and 1C cycle rates using a pulse discharge profile mimicking a real system. Cells at the 1C cycle rate continued to function well after 6000 cycles, while the 10C cells reached end of life after 1175 cycles. The 4P1S array was also cycled to end of life (750 cycles), a reduction of 36% in lifetime compared to single-cell data. The imaginary impedance values at f_{SOH} are found to be converging to a relatively narrow impedance range of 14 mΩ at 10C, and 18 mΩ at 1C, validating the derivation of the f_{SOH}. The cells at 10C also show a measurable increase in the 1-kHz ESR on the real axis, with a median increase of 2 mΩ after 600 cycles. When compared to the data described in,[1,2] it appears the physical size of the cell has a direct effect on the f_{SoH} for that form factor, as the 18650 has an identified frequency of 316 Hz compared to the 158 Hz identified in our work. Further research needs to be conducted with 18650 $LiFePO_4$ and 26650 $LiCoO_2$ cells to determine the full extent of the influence of form factor versus chemistry.

Acknowledgments

Work supported by the US Office of Naval Research and US Naval Research Laboratory Base Program on ONR Contract No. N00173-13-D6015 and N00173-10-C6012. DISTRIBUTION STATEMENT A: Approved for public release; distribution is unlimited.

References

1. N. S. Spinner, C. T. Love, S. L. Rose-Pehrsson, and S. G. Tuttle, *Electrochimica Acta*, **174**, 488 (2015).
2. C. T. Love, M. B. V. Virji, R. E. Rocheleau, and K. E. Swider-Lyons, *Journal of Power Sources*, **266**, 512 (2014).
3. S. S. Zhang, K. Xu, and T. R. Jow, *Journal of Power Sources*, **115**, 137 (2003).
4. G. Park, H. Nakamura, Y. Lee, and M. Yoshio, *Journal of Power Sources*, **189**, 602 (2009).
5. S.-i. Tobishima and J.-i. Yamaki, *Journal of Power Sources*, **81**, 882 (1999).
6. J. P. Schmidt, T. Chrobak, M. Ender, J. Illig, D. Klotz, and E. Ivers-Tiffee, *Journal of Power Sources*, **196**, 5342 (2011).
7. A. Jossen, *Journal of Power Sources*, **154**, 530 (2006).
8. C. Wang, A. J. Appleby, and F. E. Little, *Journal of Electroanalytical Chemistry*, **497**, 33 (2001).
9. F. Nobili, F. Croce, B. Scrosati, and R. Marassi, *Chemistry of Materials*, **13**, 1642 (2001).
10. X. Y. Qiu, Q. C. Zhuang, Q. Q. Zhang, R. Cao, P. Z. Ying, Y. H. Qiang, and S. G. Sun, *Phys Chem Chem Phys*, **14**, 2617 (2012).
11. F.-M. Wang, H.-Y. Wang, M.-H. Yu, Y.-J. Hsiao, and Y. Tsai, *Journal of Power Sources*, **196**, 10395 (2011).
12. T. Momma, M. Matsunaga, D. Mukoyama, and T. Osaka, *Journal of Power Sources*, **216**, 304 (2012).
13. X. Gong, R. Xiong, and C. C. Mi, *Ieee T Ind Appl*, **51**, 1872 (2015).
14. R. Gogoana, M. B. Pinson, M. Z. Bazant, and S. E. Sarma, *Journal of Power Sources*, **252**, 8 (2014).
15. Z. C. Feng and Y. Zhang, *International Journal of Energy Research*, **38**, 813 (2014).
16. M. Dubarry, C. Truchot, and B. Y. Liaw, *Journal of Power Sources*, **219**, 204 (2012).
17. M. Dubarry, V. Svoboda, R. Hwu, and B. Yann Liaw, *Electrochemical and Solid-State Letters*, **9**, A454 (2006).
18. C. T. Love and K. Swider-Lyons, *Electrochemical and Solid-State Letters*, **15**, A53 (2012).
19. C. T. Love, K. Swider-Lyons, and C. J. Patridge, *Meeting Abstracts*, **MA2012-02**, 1041 (2012).
20. T. Osaka, D. Mukoyama, and H. Nara, *Journal of the Electrochemical Society*, **162**, A2529 (2015).